Available online at www.sciencedirect.com
ScienceDirect
International Journal of Heat and Mass Transfer 51 (2008) 2506–2518
International Journal of HEAT and MASS TRANSFER
www.elsevier.com/locate/ijhmt

Consideration of heat transfer in pore network modelling of convective drying

V.K. Surasani, T. Metzger *, E. Tsotsas

Thermal Process Engineering, Otto-von-Guericke-University, Universitaetsplatz 2, 39106 Magdeburg, Germany

Received 19 April 2007; received in revised form 5 July 2007
Available online 27 September 2007

Abstract

The influence of heat transfer on the drying behaviour of capillary porous media saturated with water is studied. To overcome the limitations of continuum approaches, a pore network model based on statistical physics and invasion percolation is used. The presented non-isothermal model is the first of its kind to describe free evolution of temperatures in convective drying. Gas-side mass transfer is modelled by a discretised boundary layer. Model assumptions are purely conductive heat transfer in the network and negligible viscosity. Vapour condensation is partially modelled. Simulations are conducted on two-dimensional square lattice networks. Overall drying rates and corresponding evolution of phase distributions and temperature fields are presented for mono- and bi-modal pore structures. The influence of heat transfer on phase distributions and drying behaviour is discussed in comparison with isothermal simulations.

Keywords: Porous structure; Drying kinetics; Phase distributions; Temperature fields; Diffusive boundary layer; Invasion percolation

1. Introduction

Drying of porous media imposes a challenging modelling task since it involves mass, momentum and heat transfer in a three-phase (solid, liquid and gas) system. Classical models are based on homogenization [1] or volume averaging techniques [2] and treat the porous medium as a fictitious continuum describing its behaviour at the macroscale. The macroscale is defined by the length over which the system can be considered as homogeneous. Every continuous model requires the knowledge of effective transport parameters, which are averaged properties and need to be found by fitting to experimental data or theoretically by assumptions about the pore space. Many of the past theories attempt to derive effective parameters of porous media by some simple representation of the pore space, often as a bundle of capillary tubes [3]. However, these models will fail when the interconnectivity of pore space or fluid phase plays a major role. It is unclear, how fractal or cluster formations in two-phase flow can be described in a continuous way. In general, drying in porous media is a random process [4] due to stochastic geometry of the void space and transport steps that can hardly be accounted by any continuous model.

Discrete models using a network representation of pore structure and based on statistical physics, i.e. percolation theory, are particularly suited where the continuous approach fails [5]. The geometry of void space in porous media is represented as a network of pores connected with throats. Various geometrical shapes have been adapted for pores and throats in literature. Spherical pore bodies may be considered to contain the entire void space of the network, with the throats acting only as conductors [6]. Alternatively, the entire void space may be attributed to either bi-conical [7] or uniform cross section [8] throats, regarding the pores as merely the volumeless nodes of the network. Pore network modelling was first developed for drying by Daian and Saliba [9] in order to describe moisture migration in porous media. Nowicki et al. [7] worked on drying of porous media, including viscous effect in the liquid

* Corresponding author. Tel.: +49 391 6711362; fax: +49 391 6711160.
E-mail address: thomas.metzger@ovgu.de (T. Metzger).

0017-9310/$ - see front matter © 2007 Elsevier Ltd. All rights reserved.
doi:10.1016/j.ijheatmasstransfer.2007.07.033

Nomenclature

A	area of cross section (m^2)
c_p	specific heat capacity (J/kg/K)
g	mass transfer conductance (kg/s)
H	enthalpy content (J)
L	length of throat (m)
$\widetilde{M}$	molar mass (kg/kmol)
$\dot{M}$	mass flow rate (kg/s)
N	number of pores/clusters (–)
P	pressure (Pa)
$\dot{Q}$	heat flow rate (W)
$\widetilde{R}$	ideal gas constant (J/kmol/K)
r	throat radius (m)
S	saturation (–)
T	temperature (K)
t	time (s)
V	volume (m^3)
W	network thickness (m)
Δh	specific phase change enthalpy (J/kg)

Greek symbols

α	heat transfer coefficient ($W/m^2/K$)
β	mass transfer coefficient (m/s)
γ	surface tension (N/m)
δ	vapour diffusivity (m^2/s)
κ	thermal diffusivity (m^2/s)
λ	thermal conductivity (W/m/K)
ν	kinematic viscosity (m^2/s)
ρ	density (kg/m^3)

Subscripts/superscripts

BL	boundary layer
c	capillary
C	condensation
ev	evaporation
g	gas
i or j	pore or node
ij	throat connecting pores i and j
l	liquid
lm	number of menisci
nc	cluster number
s	solid
T	total network
v	vapour
*	equilibrium

phase, to determine effective transport parameters; Yiotis et al. [6] studied the effect of viscosity in both the gas and the liquid phase for drying of porous rocks. Prat et al. [8] investigated the stabilization of the drying front in the presence of gravity. A similar stabilization has been observed for viscous effects in the liquid [10]. Micro-model experiments have shown similar invasion patterns as the simulations [11]. However, simulated drying rates are greatly underestimated [12]. Film flows, which can contribute largely to the first drying period [13,14] can explain the difference between experimental and numerically simulated drying rates. Segura and Toledo [15,16] studied pore scale models based on the previous work by Prat [8].

Most of the above work on pore networks studied the influence of physical effects, i.e. capillary pumping, viscous flow, film flows and gravity, on overall drying behaviour under isothermal conditions. Metzger et al. [10,17], based on models similar to those of Prat, describe the influence of pore structure on drying behaviour also under isothermal conditions.

Despite of significant progress in the last decade, most pore network drying models are isothermal and, therefore, applicable only to low drying rates [5]. In convective drying, however, energy needed for evaporation is supplied to the moist product by dry airflow. Simultaneously, evaporated moisture is released to the ambient medium, making drying a coupled heat and mass transfer problem. Failing consideration of this coupling may lead to wrong results for drying kinetics. Until now, very little work has been done concerning the inclusion of heat transfer into pore network modelling. To our knowledge, only the influence of temperature gradients – which were imposed onto the drying product – has been investigated by Plourde and Prat [18], Huinink et al. [19]. Temperature dependence of liquid surface tension and equilibrium vapour pressure were accounted for and respective gradients made responsible for stabilization or destabilization of the drying front and for changes in drying rates. However, product temperature did not evolve freely as corresponding to convective drying boundary conditions.

As a step towards a complete pore network model, the present paper introduces heat transfer to the existing isothermal model version [20] that neglects viscous effects. The solid is considered non-hygroscopic, thus neglecting adsorption phenomena. Heat transfer in the network is assumed to take place only by conduction. Heat transfer parameters, i.e. thermal conductivity and heat capacity, are only functions of saturation. The non-isothermal model for convective drying and the numerical solution are presented first. Then, simulation results of drying kinetics, temporal evolution of phase distributions (cluster formation) and temperature fields are discussed for mono- and bi-modal pore size distributions.

2. Non-isothermal modelling

The non-isothermal model developed and implemented in the present work is an extension of an isothermal pore network drying model, which is based on the work of Prat [21] and includes discrete modelling of the boundary layer

[17]. Since, pore network models take geometry into account, the data structure for representing geometry will be discussed briefly before presenting model equations for heat and mass transfer.

2.1. Pore network

Void space in the porous medium is regarded as a network of cylindrical throats with randomly distributed radius connected by pore nodes without volume. In this paper, we restrict ourselves to two-dimensional square networks. Fig. 1 shows such a network of pores and throats and how is associated a control volume to each pore. As known from literature, the invasion behaviour of two-dimensional networks is slightly different to that of three-dimensional networks due to the lower connectivity of the pore space, e.g. [21]. The proposed algorithm is general enough to be applied to three-dimensional networks but still faces computational limits.

Throughout the paper white space (inside throats) represents the air and vapour phase, and black space stands for liquid. Initially, the network is fully saturated with water and has room temperature (20 °C). Only the top edge of the network is open to evaporation and subjected to heating or cooling; the remaining faces are impervious to heat and mass transfer.

2.2. Boundary layer model

For drying, the network is subjected at its open edge to lateral air flow with velocity u, bulk vapour pressure $P_{v,\infty}$ and bulk temperature T_∞. To realistically describe the drying kinetics, especially the first drying period with its constant drying rate, it is necessary to model the boundary layer in a discretised way, extending the network into the gas by additional nodes (see Fig. 2).

Assuming laminar flow over the network, the Sherwood number describing mass transfer is given by

$$Sh = \frac{\beta L_T}{\delta} = 0.664 Re^{1/2} Sc^{1/3} \tag{1}$$

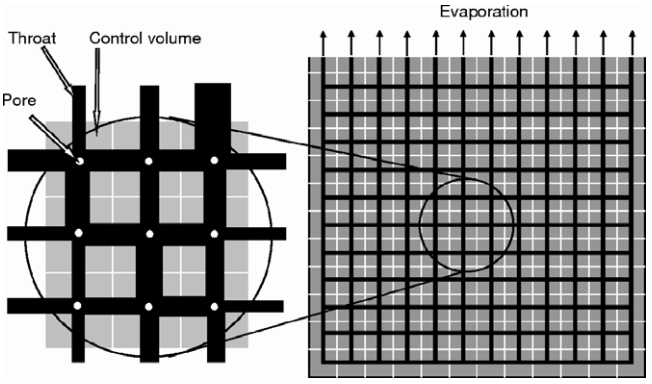

Fig. 1. Schematic representation of the porous medium by a 2D square network.

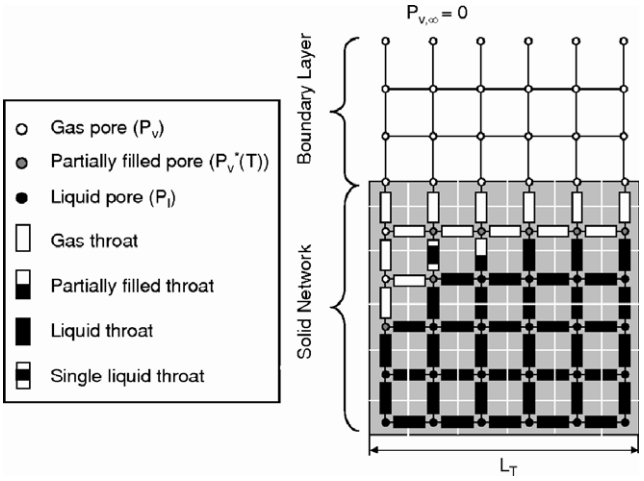

Fig. 2. Illustration of boundary layer over the network and state of pores and throats at some time during the drying process.

with Reynolds number $Re = uL_T/\nu_g$ and Schmidt number $Sc = \delta/\nu_g$. Here, β is mass transfer coefficient, L_T network length, δ vapour diffusivity and ν_g kinematic viscosity of the gas. However, Eq. (1) is derived for a plate at uniform partial pressure which is not necessarily fulfilled for drying porous medium (see [22]). From this, boundary layer thickness and the number of additional vertical nodes N_{BL} are obtained as

$$\varepsilon = \frac{\delta}{\beta} = N_{BL} L, \tag{2}$$

where the distance between nodes L is the same as the length of network throat. Vapour pressure of bulk air (here $P_{v,\infty} = 0$) provides the boundary condition for the extended network. Heat transfer between bulk air and network surface is described by a heat transfer coefficient α, which can be calculated by

$$\alpha = \beta \frac{\lambda_g}{\delta} \left(\frac{Pr}{Sc}\right)^{\frac{1}{3}} \tag{3}$$

based on the analogy between heat and mass transfer. Here λ_g is thermal conductivity of the gas and $Pr = \delta/\kappa_g$ is Prandtl number with thermal diffusivity κ_g. Fig. 2 illustrates the structure of the network and the boundary layer in the process of drying. For clarity, imaginary spherical pores are shown.

2.3. Pore and throat conditions

The state of throats plays a vital role in determining transport mechanisms during drying. Throats contain all void space and serve as the conductors in the network, carrying heat and mass flows due to temperature and vapour or liquid pressure gradients between the pores. Throats can be classified as gas throats, liquid throats and partially filled throats based on their saturation S_{ij} (see Fig. 2). The type of transport in the throats is also determined by saturation. If throat saturation S_{ij} is unity, liquid flow will

take place due to capillary pumping; if S_{ij} is equal to zero, vapour will be transferred by diffusion; and if S_{ij} is between 0 and 1, combined liquid flow, evaporation at the meniscus, and vapour diffusion will take place in a throat.

Pores represent the structural parameters of the void space and the state variables in each control volume. Structural parameters, constant in time, are the spatial positions of pores and their relative positions with respect to other pores and throats. State variables are saturations S_i, temperatures T_i, vapour pressures $P_{v_{i,i}}$ (eventually also total gas pressure) and liquid pressures $P_{l,i}$. Pore saturation S_i is determined by its neighbour throat saturations S_{ij}. If all neighbour throats are full, saturation is unity (liquid pore); and it is zero (gas pore) if all neighbour throats are empty. In general, pore saturation is equal to the fraction of full or partially filled throats ($0 \leqslant S_i \leqslant 1$). In partially filled pores, we assume equilibrium vapour pressure (see Fig. 2), which sets the boundary condition for evaporation during the drying process. Nodes in the boundary layer are always at unknown vapour pressures.

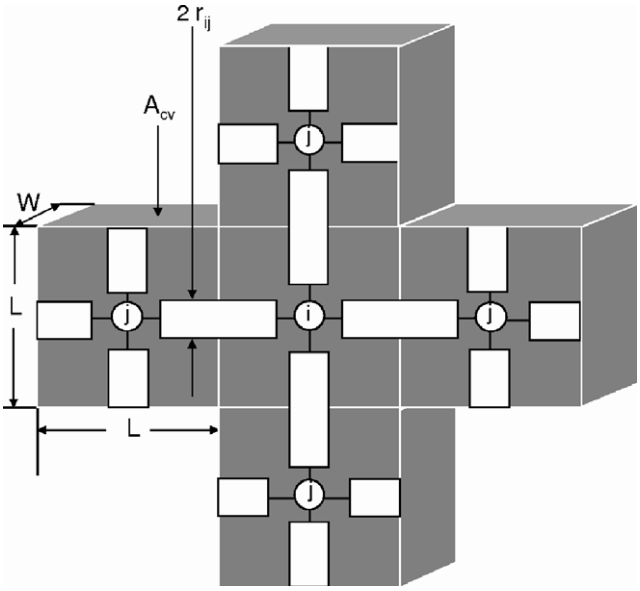

Fig. 3. Control volume i with neighbours j and exchange areas.

2.4. Heat and mass transfer relations

The implemented model is based on the following assumptions:

1. Constant boundary layer thickness;
2. constant total pressure in the gas phase;
3. quasi-stationary diffusive vapour transport;
4. negligible viscosity of liquid (capillary forces dominate over viscous forces);
5. heat transfer in the network only by conduction;
6. local thermodynamic equilibrium in each control volume.

The vapour flow rate between two gas pores due to vapour pressure gradients is given by Stefan's law as

$$\dot{M}_{v,ij} = -A_{ij}\frac{\delta}{L_{ij}}\frac{P\widetilde{M}_v}{\widetilde{R}T}\ln\left(\frac{P-P_{v,i}}{P-P_{v,j}}\right), \tag{4}$$

where $\widetilde{M}_v$ is molar mass of vapour, $\widetilde{R}$ ideal gas constant and T absolute temperature. Eq. (4) also describes the vapour flow rate between two nodes in the boundary layer, only the cross sectional area A_{ij} must be chosen accordingly. It is

$$A_{ij} = \pi r_{ij}^2 \quad \text{for network,} \tag{5}$$

$$A_{ij} = LW \quad \text{for boundary layer,} \tag{6}$$

where r_{ij} is throat radius and W network thickness in the third dimension (see Fig. 3). Since we neglect the overlap of throats at pore nodes, all throats in the network are assumed as equal in length ($L_{ij} = L$).

The liquid flow rate in the network between pores i and j due to different liquid pressures $P_{l,i}$ and $P_{l,j}$ can be calculated by Poiseuille's law as

$$\dot{M}_{l,ij} = \frac{\pi r_{ij}^4}{8\nu_l L}(P_{l,i} - P_{l,j}) \tag{7}$$

with the kinematic viscosity of water ν_l. However, Eq. (7) is not used in the present model because of the fourth assumption; instead, we apply a rule valid when viscous effects are negligible compared to capillary effects that will be discussed in Section 3.2.

Since heat transfer is only by conduction, heat flow rates due to temperature gradients are given by Fourier's law

$$\dot{Q}_{ij} = A_{cv,ij}\lambda_{ij}\frac{T_i - T_j}{L}, \tag{8}$$

where the exchange area is $A_{cv,ij} = LW$ (because both voids and solid can contribute to heat transfer). The effective thermal conductivities λ_{ij} are functions of throat saturation

$$A_{cv,ij}\lambda_{ij} = (A_{cv,ij} - \pi r_{ij}^2)\lambda_s + \pi r_{ij}^2 S_{ij}\lambda_l \tag{9}$$

with thermal conductivities of solid and liquid λ_s and λ_l, respectively. For simplicity, solid and liquid are considered as resistances in parallel, conduction in the gas is neglected. The enthalpy content H_i of control volume V_i is given by

$$H_i = V_i(\rho c_p)_i(T_i - T_{ref}), \tag{10}$$

where the total heat capacity of the control volume is

$$V_i(\rho c_p)_i = \left(V_i - \frac{L}{2}\sum_{j=1}^{4}\pi r_{ij}^2\right)(\rho c_p)_s + \frac{L}{2}\sum_{j=1}^{4}\pi r_{ij}^2 S_{ij}(\rho c_p)_l. \tag{11}$$

Fig. 3 shows how each control volume is represented by one pore and contains four-half throats, i.e. each throat participates in two control volumes. Liquid of partially filled throats are equally distributed to neighbour pores.

From the law of conservation and the assumption of quasi-steady vapour transport, total mass flow from any gas pore is equal to zero. By applying Eq. (4) to gas pore i, we obtain

$$\sum_{j=1}^{4} \dot{M}_{v,ij} = \sum_{j=1}^{4} A_{ij} \frac{\delta}{L} \frac{P\widetilde{M}_v}{\widetilde{R}T} \ln\left(\frac{P - P_{v,i}}{P - P_{v,j}}\right) = 0, \tag{12}$$

where $\dot{M}_{v,ij}$ is the mass flow rate of vapour. For partially saturated pores the vapour balance can be written as

$$\sum_{j=1}^{4-\mathrm{lm}} \dot{M}_{v,ij} = \sum_{j=1}^{\mathrm{lm}} \dot{M}_{ev,ij} \tag{13}$$

with evaporation or condensation rates $\dot{M}_{ev,ij}$ in the connected meniscus throats (lm). Similarly, for a model with liquid viscosity, we have for the liquid pores

$$\sum_{j=1}^{4} \dot{M}_{l,ij} = \sum_{j=1}^{4} \frac{\pi r_{ij}^4}{8 v_l L} (P_{l,i} - P_{l,j}) = 0 \tag{14}$$

The boundary conditions to this set of equations are given at the menisci and must be found by an iterative algorithm (Metzger et al., [10]). If a meniscus is moving, a pressure boundary condition of first kind is applied ($P_{l,ij} = P - P_{c,ij}$); if it is stationary, the local evaporation rate gives a boundary condition of second kind ($\dot{M}_{l,ij} = \dot{M}_{ev,ij}$). The dynamic energy balance over the control volume can be derived from Eqs. (8) and (10) as

$$V_i (\rho c_p)_i \frac{\mathrm{d}T_i}{\mathrm{d}t} = -\sum_{j=1}^{4} \dot{Q}_{ij} - \Delta h_{v,i}(T_i) \sum_{j=1}^{\mathrm{lm}} \dot{M}_{ev,ij}, \tag{15}$$

where $\Delta h_{v,i}(T_i)$ is phase change enthalpy (absolute value). The mass flow rate $\dot{M}_{ev,ij}$ is positive for evaporation and negative for condensation. The meniscus position is used to allocate heat sink/source to a control volume.

2.5. Coupling of heat and mass transfer

The interaction between heat and mass transfer influences considerably the drying process, particularly at the phase boundaries in the network. At an evaporating meniscus, the vapour takes up the enthalpy of evaporation and the liquid temperature is reduced (heat sink); likewise, we have heat sources at places of condensation. This coupling of mass transfer with heat transfer is already implemented by including rates of evaporation and condensation in the dynamic energy balance equation (Eq. (15)).

As a second major coupling effect, equilibrium vapour pressures $P^*_{v,i}(T_i)$ at the menisci are strongly temperature dependent. In the presence of a temperature field, equilibrium vapour pressure varies spatially. These vapour pressures have to be updated after each time step by use of an Antoine equation.

At the same time, due to temperature differences, gradients in surface tension γ will develop and instigate gradients in capillary pressure

$$P_{c,ij} = \frac{2\gamma(T_{ij})}{r_{ij}} \tag{16}$$

that contribute to liquid flow additionally to the effect of different throat radii.

3. Numerical solution

In drying of porous media, capillary pressure gradients exist and cause liquid flow by capillary pumping. Viscous forces will counteract capillary forces and always stabilize the receding drying front, because they reduce the distance over which liquid can be pumped at a given rate [10]. As we will see the assumption of zero liquid viscosity leads to a discrete way of solving the model for liquid transport. The continuous conservation equations for vapour and energy, Eq. (12) and Eq. (15), have to be solved together with the discrete model part that describes liquid transport due to capillary pumping. The quasi-steady vapour balances of Eq. (12) are solved for the current boundary conditions at the meniscus throats. Dynamic energy balances Eq. (15) are solved by an explicit scheme using the current phase distribution and temperature field.

3.1. Vapour transport

Rewriting Eq. (12) for each pore of unknown vapour pressure i and introducing mass transfer conductances g_{ij} leads to

$$\sum_{j=1}^{4} g_{ij}(lp_i - lp_j) = \sum_{j=1}^{4} g_{ij} lp^*_j, \tag{17}$$

where the logarithmic pressure differences are

$$lp_i = \ln(P - P_i)$$
$$lp_j = \begin{cases} \ln(P - P_j) & \text{for } S_j = 0 \\ 0 & \text{for } 0 < S_j < 1 \end{cases} \tag{18}$$

The right hand side of Eq. (17) gives the boundary conditions at the liquid–gas interface and at the edge of the gas-side boundary layer as

$$lp^*_j = \begin{cases} 0 & \text{for } S_j = 0 \\ \ln(P - P^*_{v,j}(T_j)) & \text{for } 0 < S_j < 1 \\ \ln(P - P_{v,\infty}) & \text{edge of boundary layer} \end{cases} \tag{19}$$

Applying Eq. (17) to all gas pores in network and boundary layer at a given time, forms the linear system

$$\mathbf{G} \bullet \mathbf{LP} = \mathbf{LP}^* \tag{20}$$

where $\mathbf{G}$ is a sparse symmetric matrix containing mass transfer conductances g_{ij}, $\mathbf{LP}$ represents the unknown vector of lp_i and $\mathbf{LP}^*$ the vector of boundary conditions. Eq. (20) is solved using the conjugate gradient method (CGM); then, vapour flow rates $\dot{M}_{v,ij}$ can be calculated from Eq. (4).

3.2. Liquid transport

The assumption of negligible viscous effects implies that, in each cluster, liquid can be pumped from the throat with the highest liquid pressure to all other menisci at their

respective rates of evaporation, and that only this one throat will empty. So, it is necessary to identify the throat with the lowest capillary pressure $P_{c,ij}$ (i.e. highest liquid pressure $P_{l,ij}$) for the current temperatures at each time step.

Fig. 4 shows liquid transport in a single cluster with a moving meniscus (MM) throat; all remaining menisci are stationary. For each time step, the mass lost due to evaporation from all menisci in the cluster must be removed from the throat with the lowest capillary pressure (shaded volume). For isothermal conditions, this will always be the throat with largest r_{ij} in a cluster (see Eq. (16)).

When a throat has emptied completely, throat and pore saturations must be updated, changing the linear system of Eq. (20). Therefore, we must introduce a mass transfer time step $\Delta t_{m,nc}$ for each cluster nc, which is calculated as the ratio of liquid mass left in the MM throat and sum of evaporation rates at the menisci of the cluster:

$$\Delta t_{m,nc} = \frac{\rho_l V_{MM,nc}}{\sum_{j=1}^{mt} \dot{M}_{ev,ij,nc}}. \tag{21}$$

Here, mt is the number of evaporating throats in a cluster.

3.3. Condensation

If the system is considered to be non-isothermal, spatial temperature gradients build up over the network during the drying process. Since equilibrium vapour pressure is highly sensitive to the temperature, equilibrium vapour pressure gradients will develop. At the same time, capillary pressure gradients may cause splitting of the continuous liquid phase into disconnected wet patches (liquid clusters) at different temperatures. Due to the above phenomena, vapour evaporating from hot clusters or single throats may move against the main direction of mass flow and condense on cold clusters or single throats (vapour back diffusion may take place instead of the escape of vapour from the top surface).

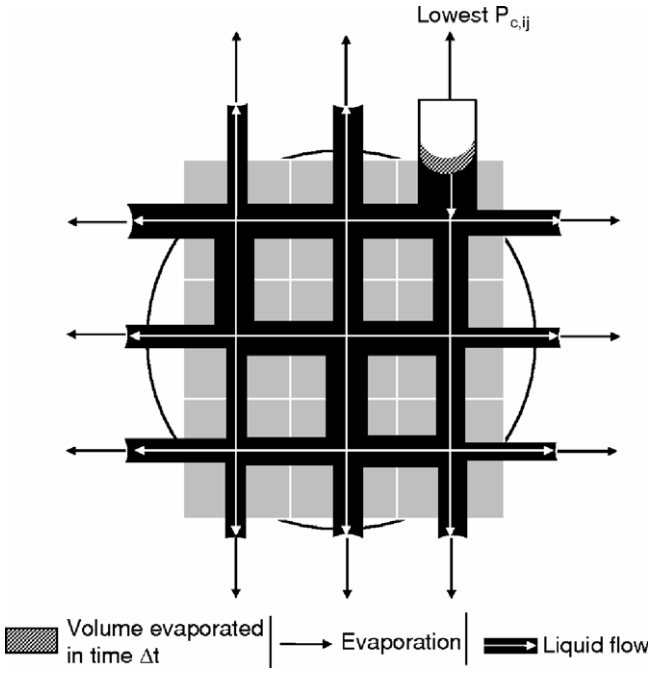

Fig. 4. Liquid flow due to capillary pumping as well as stationary and moving menisci for a single cluster.

The effect of condensation is fully included in heat transfer, Eq. (15), but it is only partially accounted for in mass transfer. For each cluster or single liquid throat, the net phase change rate is computed as the sum of all meniscus evaporation/condensation rates. If there is net evaporation in a cluster, the previously described algorithm (Section 3.2) can be used. For clusters with net condensation, we can either refill a partially emptied throat (MM throat) with mass transfer time step

$$\Delta t_{m,nc} = -\frac{(1 - S_{MM})\rho_l V_{MM,nc}}{\sum_{j=1}^{mt} \dot{M}_{ev,ij,nc}} \tag{22}$$

or we have to neglect condensation because imbibition of completely emptied throats is not included in the model. Therefore, not all condensing vapour can be accommodated but the committed error can be assessed because the true condensation rates are known. When simulation results will be presented in Section 4, the error on condensation rates will also be discussed.

3.4. Cluster labelling

One of the main advantages of discrete network models over continuous models is that the former can describe the disintegration of the liquid phase into disconnected clusters, while the latter are limited to smooth variations of pore saturation. In the isothermal case, clusters will form due to random throat size distribution. In the presence of thermal gradients, surface tension gradients may cause additional capillary pressure differences. To describe correctly liquid transport in the network, the connectivity of the liquid phase must be known, so that cluster labelling of throats is necessary. To this purpose, the Hoshen–Kopelman algorithm (well documented in literature) can be used [23,24].

Fig. 5 shows how a mass transfer time step $\Delta t_{m,nc}$ computed by Eq. (21) or Eq. (22) is associated to every cluster and every isolated throat. From these, the minimum must be chosen as the mass transfer time step of the network $\Delta t_{m,min}$.

3.5. Dynamic heat transfer by explicit scheme

Heat transfer is continuous in the presence of thermal effects, even though mass transfer naturally imposes discrete time steps (by the emptying of throats). Therefore, a different time discretisation will be necessary. For the updating of temperature fields in the entire network, dynamic energy balance was implemented in an explicit

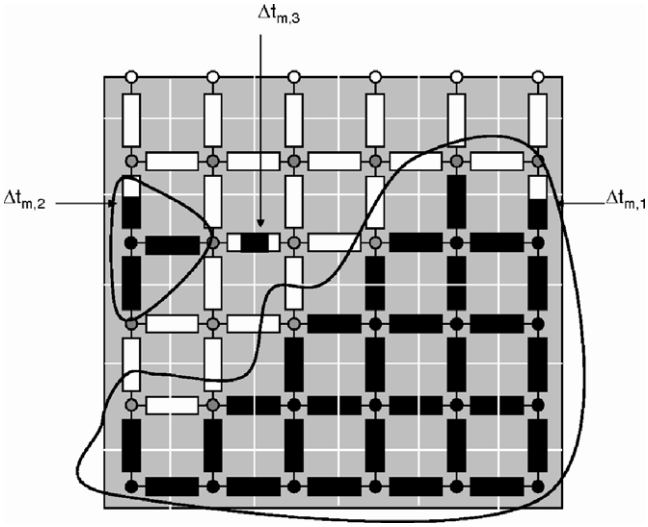

Fig. 5. Cluster formation during drying and different mass transfer time steps.

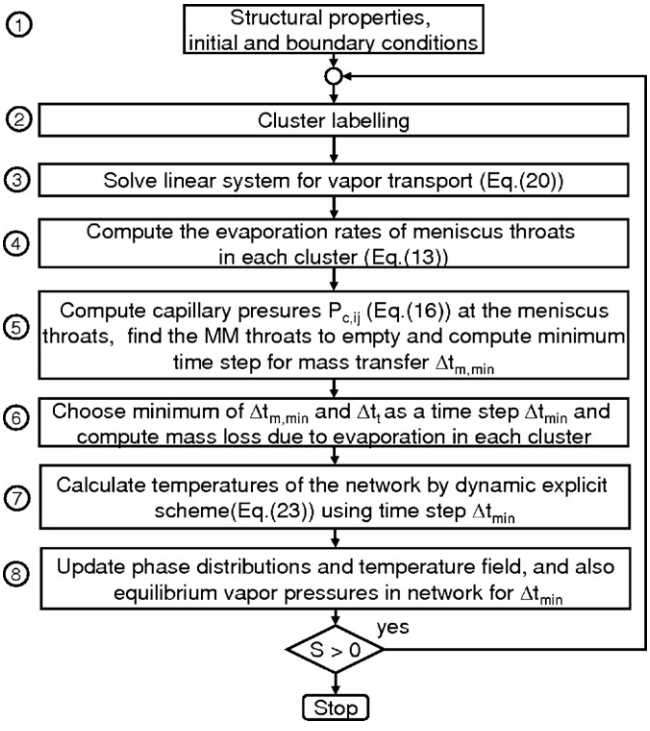

Fig. 6. Flow sheet for the drying algorithm.

scheme. By substituting Eq. (8) into Eq. (15) and integrating this equation over the thermal time step Δt_t we obtain

$$T_i|_{t+\Delta t} = T_i + \frac{\Delta t_t}{V_i(\rho c_p)_i}\sum_{j=1}^{4}\left(-A_{cv,ij}\lambda_{ij}\frac{T_i - T_j}{L} - \Delta h_v(T_i)\dot{M}_{ev,ij}\right). \quad (23)$$

The stability of the explicit method is only guaranteed if the thermal time step fulfils the condition

$$\Delta t_t < \frac{(\rho c_p)_i L^2}{\sum_j \lambda_{ij}} \quad (24)$$

for all control volumes i. If this critical value is exceeded, physically unrealistic results like negative temperatures may be observed. The major disadvantage of the explicit scheme is the small time step that causes large computational times.

3.6. Drying algorithm

Fig. 6 illustrates the numerical solution of the non-isothermal network drying model. First, the data structures describing the pore grid of network and boundary layer must be formed from network size (e.g. 51 × 51); additionally drying air velocity, initial and boundary conditions are set (step 1). After cluster labelling (step 2), the linear system for vapour transport (Eq. (20)) is solved (step 3) and the evaporation rates at each meniscus are computed (step 4). Then, from the capillary pressures $P_{c,ij}$ in meniscus throats,

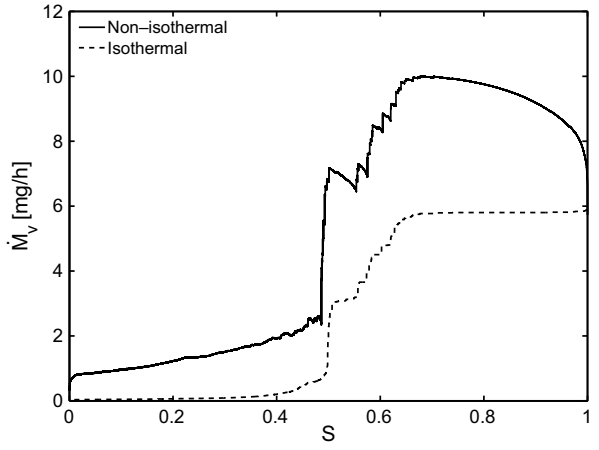

Fig. 7. Isothermal and non-isothermal drying rate curves for bi-modal network.

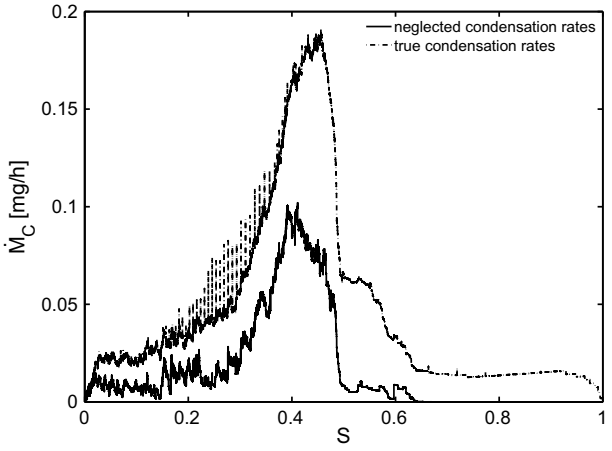

Fig. 8. Actual and neglected condensation rates in the non-isothermal model due to temperature gradients.

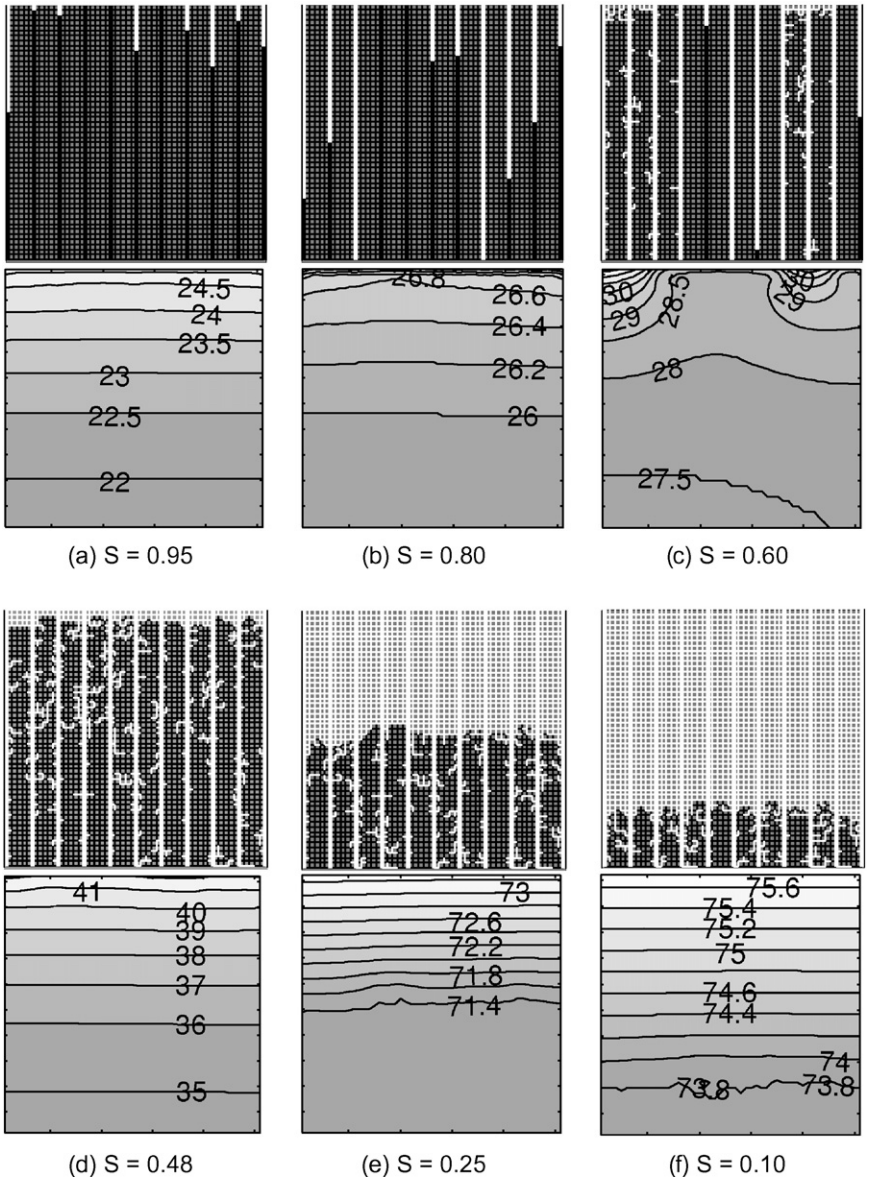

Fig. 9. Evolution of phase and temperature distributions for bimodal case network (saturations are indicated).

the MM throat is identified for each cluster, and the minimal mass transfer time step $\Delta t_{m,min}$ calculated (step 5). The time step Δt_{min} is chosen as the minimum out of mass transfer time step $\Delta t_{m,min}$ and heat transfer time step Δt_t, which obeys stability criteria of Eq. (24) (step 6). The mass loss due to evaporation is computed for the time step Δt_{min}.

Next, the new temperature field is computed by using Eq. (23) for same time step (step 7). Finally, phase distributions (pore and throat saturations) and temperature fields (as well as temperature dependent variables) are updated (step 8). The procedure will be repeated in a loop until all water is removed from the network.

4. Simulation results

The results presented in this section have been obtained for networks of size 51×51 with mono- and bi-modal throat size distribution. The radius of throats is randomly varied according to the normal number density function

$$f(r) = \frac{1}{\sqrt{2\pi}\sigma_0} e^{\frac{(r-r_0)^2}{2\sigma_0^2}} \tag{25}$$

with mean r_0 and standard deviation σ_0. A mean radius of 40 μm and a standard deviation of 2 μm are used for the mono-modal network (see Fig. 13 for realization). In the bi-modal pore network, radii from a distribution with 100 ± 5 μm are applied to every fifth vertical throat, leaving the remaining throats as of mono-modal network (Fig. 9). Throat length is 500 μm for all networks.

Initially, the network is saturated with water and has a uniform temperature of 20 °C. The heat transfer parameters of the solid are chosen as for glass: $(\rho c_p)_s = 1.7 \times 10^6$ J/(m^3 K) and $\lambda_s = 1$ W/(m K). Bulk air is at

$T_\infty = 80$ °C, has zero moisture content and velocity such that the boundary layer contains 7 nodes ($\beta = 7.3$ mm/s).

Fig. 7 shows the drying kinetics for the bi-modal pore network as evaporation rate $\dot{M}_v$ versus network saturation S. Both the isothermal and the non-isothermal curve start at the same rate. The initial warming-up to constant drying conditions can be clearly seen in the non-isothermal process. The constant rate period extends for both curves to a saturation of approximately 0.6, i.e. almost until all the macro-throats (43% of volume) are emptied.

As explained above, the order of emptying of throats is determined by capillary pressure. In the isothermal model, it depends on the throat radius alone since temperature is constant throughout the network. In the non-isothermal model, the order of emptying may also be influenced by surface tension at the menisci (Eq. (16)). However, at the beginning, influence of temperature on capillary pressure via surface tension is negligible and the macro-throats will empty first because here capillary pressure is always lowest. Liquid will be pumped through the micro-throats to the network surface so that the surface can stay almost completely wet down to relatively low overall saturations. Lateral vapour transfer in the boundary layer assures a constant drying rate [17].

The evaporation rate drops drastically when the surface starts to dry out after all macro-throats are emptied. Short quasi-constant rate periods can be observed in this falling rate period in isothermal drying when – due to random radius distribution – throat saturation near the surface stays unchanged while internal throats empty. In the case of non-isothermal modelling, during these short periods the surface will heat up and evaporation rate increases, until another near surface throat empties; then, drying rate drops to a lower value in both model versions.

Fig. 8 shows the condensation rate $\dot{M}_C$ plotted against overall network saturation in two forms; true condensation rate and neglected condensation rate. The neglected condensation rate corresponds to the error by un-accommodated condensing vapour as explained in Section 3.3. In the first drying period, the error on condensation rate is zero. There is condensation at inner network throats but it can be compensated because clusters are still big of size; therefore, capillary flow to surface menisci, evaporating at higher rates, is not yet interrupted. Consequently, clusters as a whole are evaporating and no error is committed. The formation of relatively small clusters in the second drying period may cause net condensation in clusters, which cannot fully be accounted for. The amount of vapour condensed during the entire drying process is 2.17% of the initial amount of water present in the void space; however, only 0.90% of the initial water is neglected. This shows that the effect of condensation on overall behaviour of the drying curve can be neglected for the given example.

Fig. 9 shows the evolution of phase distributions and temperature fields at different overall saturations of the network. The situation of Fig. 9a ($S = 0.95$) is located within the warming-up period, when temperature rises towards the wet bulb temperature (see Figs. 7 and 10). Fig. 9b and c correspond to the constant rate period in which almost uniform temperature fields exist and only macro-throats will empty. Surface throats empty between $S = 0.6$ and 0.48 (Fig. 9c and d). In this period, larger temperature gradients develop and network temperature starts to rise drastically. At the same time, drying rate drops, as can be clearly seen from the sudden change of slope for the saturation curve of Fig. 10. After all the macro-throats have been emptied, a drying front recedes (see transition from Fig. 9d–f) towards the bottom of the network. This increases the resistance to mass transfer. However, rising temperatures cause, at the same time, higher driving forces for vapour diffusion. Due to the latter effect, evaporation rates are much larger than according to the isothermal model in this region (Fig. 7).

Fig. 10 illustrates the variation of temperature at the top of the network (T_{max}), temperature at the bottom of the network (T_{min}), and network saturation S with time. Fig. 11 shows the number of clusters formed N_{nc} and network saturation S with time. Wet bulb temperature (25 °C) is obtained approximately at the end of the first drying period. Only few clusters are formed during this first drying period because only macro-throats are emptying. A large increase of temperature is observed during the emptying of small surface throats. Simultaneously, the number of clusters increases drastically. The number of clusters reaches a maximum during the drastic fall of evaporation rate, decreases (with fluctuations) with time as the drying front recedes towards the bottom of the network and becomes zero at the end of the drying process.

To see the influence of pore structure, drying of a mono-modal network has been simulated for isothermal and non-isothermal conditions and compared with the results for the bi-modal network. In Fig. 12, the respective drying curves are shown. Evolution of phase distributions and temperature fields for the non-isothermal drying of the mono-modal pore network are shown in Fig. 13 for the indicated saturations.

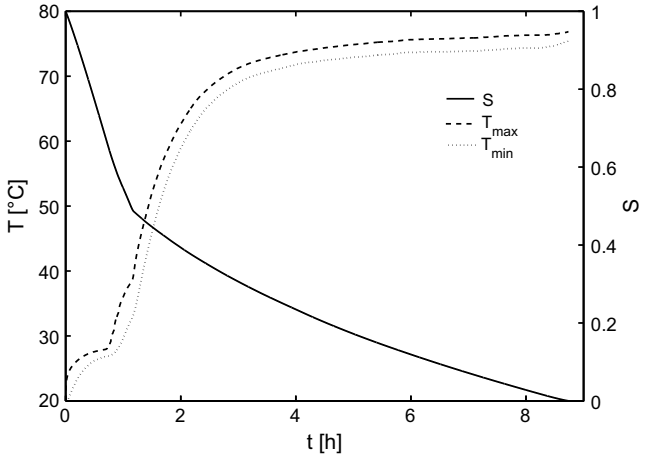

Fig. 10. Evolution of network saturation and temperature.

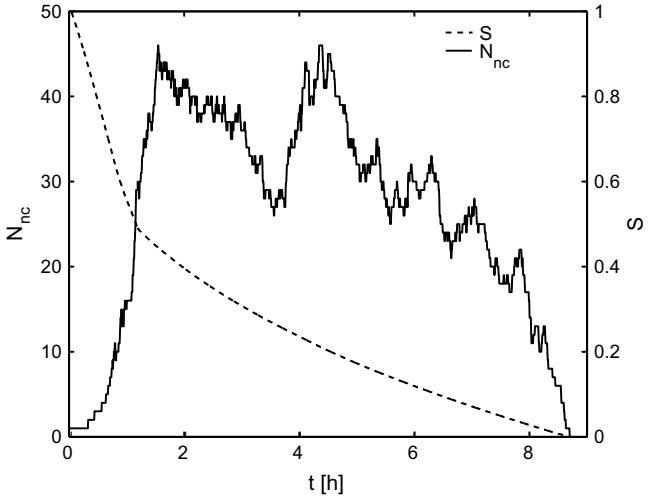

Fig. 11. Evolution of number of liquid clusters and saturation S.

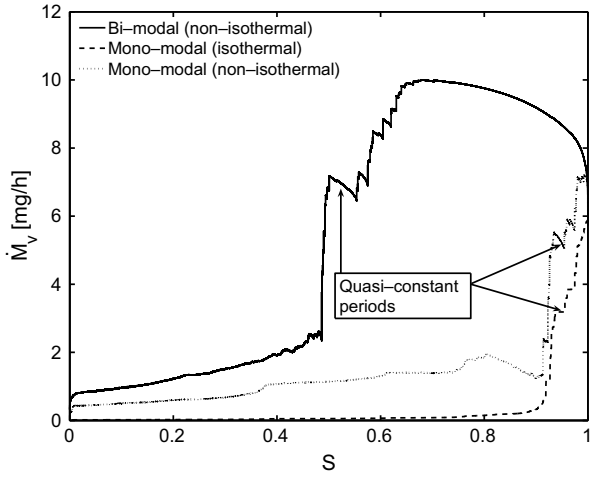

Fig. 12. Influence of pore structure on drying curve.

For all simulations, drying rate curves start at the same point because of identical initial conditions. Rapid warming leads to a sharp rise in the drying curve in both non-isothermal simulations. In the bi-modal case, the ordered emptying of macro-throats is a reason for the long constant rate period. Since macro-throats are not present in the mono-modal network, the respective first drying period is very short. Sooner or later, the gradual emptying of surface throats leads to a drastic fall of drying rates in all simulations. During this transitional period, inner throats may empty at constant wet surface fraction. This causes quasi-constant rate periods (Fig. 12). The duration of these periods depends on pore size distribution in the isothermal case. In the non-isothermal case, it depends on the dominance of capillary pressure of surface throats over that of inner throats. The temperature of the network increases in a time that is very short in comparison to total drying time. This can be seen in the temperature fields of Fig. 13a and b. A similar rise of temperature is observed at smaller overall saturations for the bi-modal network, as already discussed.

Fig. 14 gives a comparison of phase distributions obtained from isothermal and non-isothermal drying simulations for the mono-modal network. In the following, we will explain why these phase distributions are almost (but not exactly) the same. The relative change in radius of menisci throats is about 5% for the mono-modal network with a throat radius distribution of 40 ± 2 μm. The influence of temperature on surface tension γ [N/m] of water can be represented by the equation

$$\gamma[\mathrm{N/m}] = -1.704 \times 10^{-04}(T[\mathrm{K}] - 273.15) + 7.636 \times 10^{-02}, \tag{26}$$

so that the relative change in surface tension per 1 K temperature variation is approximately 0.2% (Eq. (27)). The maximal temperature gradient is about 8 K across the network and about 4 K across the drying front (see temperature fields in Fig. 14). This corresponds to a surface tension variation among the meniscus throats of maximally 0.8%. Consequently, when selecting the lowest capillary pressure throats (Eq. (17)) in a cluster, the influence of radius variation is in general larger than the influence of temperature dependent surface tension. However, when throats of very similar radius compete for the lowest capillary pressure, the influence of temperatures may have a stabilizing effect on the drying front. This stabilizing effect is due to reduction of capillary pressure with increasing temperature via surface tension under constant throat radius (Eq. (17)). Fig. 14 shows one such example of thermal stabilization at the saturation $S = 0.7$. Throats at the top of the drying front are chosen for invasion of air in the non-isothermal case, instead of throats located deeper in the network in the isothermal simulation.

5. Conclusions

In this paper, we presented a non-isothermal pore network model for the convective drying of capillary porous media. The necessity of considering heat transfer has been recognized before [18,19]. It results from the strong coupling between heat and mass transfer in the drying process, mainly due to phase change enthalpy and temperature dependent equilibrium vapour pressure, but also to temperature dependent surface tension. In the mentioned literature, however, temperature gradients were imposed on the network. Consequently, the present model is the first to describe the free evolution of temperature fields in convective drying. The model assumes dominant capillary forces and neglects both viscous forces and gravity. Vapour diffusion in the empty pore space and gas-side boundary layer is modelled as quasi-stationary; this boundary layer is discretised so that lateral vapour transfer can assure a constant rate period. Heat transfer is due to conduction, heat sinks/sources account for the evaporation/condensation of water. An algorithm to solve this model has been

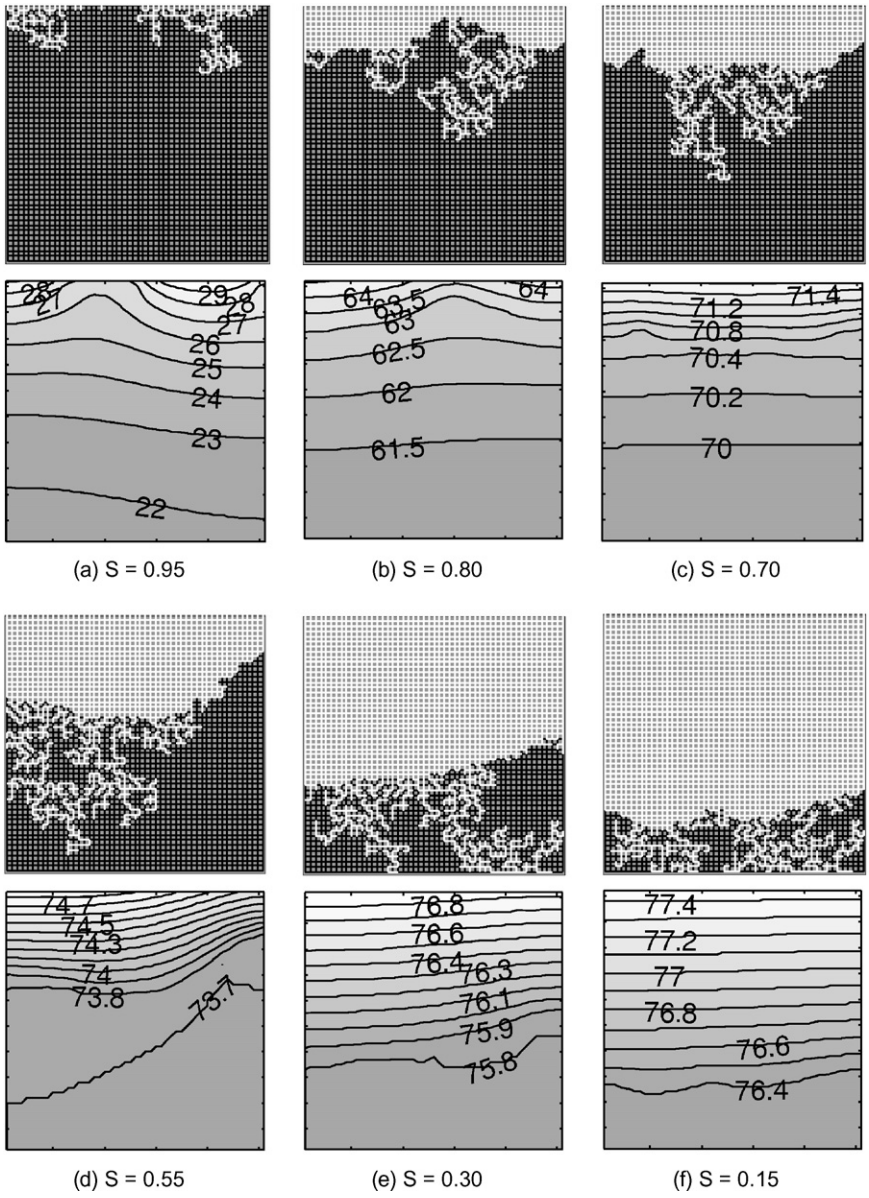

Fig. 13. Phase and temperature distributions for the non-isothermal drying of mono-modal pore network.

presented and the drying model has been applied to two-dimensional square pore networks with mono-modal and bi-modal throat radius distributions.

Characteristics of convective drying, i.e. warming-up period, constant drying rate period and falling rate period, can be observed in the simulation with a bi-modal pore network. The preferential emptying of macro-throats due to capillary pumping keeps the surface wet down to low network saturations and causes a first drying period. In the case of a mono-modal pore size distribution, after a very short warming-up period, drying rate falls drastically without a first drying period. This underlines the important role of pore structure in drying behaviour.

The influence of heat transfer on drying is mainly by an overall increase in drying rates due to the strong temperature dependency of equilibrium vapour pressure. Besides this, the invasion order of throats, which is controlled by capillary pressure differences, can be influenced by temperature gradients: capillary pressure depends both on throat radius and on temperature dependent surface tension. For the investigated case, this effect on phase distributions is relatively small, since capillary pressure differences are controlled primarily by the relative variation of throat radius. The effect is illustrated for the mono-modal pore size distribution by comparison with the isothermal simulation. For weakly disordered porous media and high temperature gradients, this thermal influence on phase patterns is expected to lead to a significant stabilization of the drying front [18,19].

In the present model version, condensation is accounted for only partially because imbibition effects would require different rules. Therefore, local condensation is only

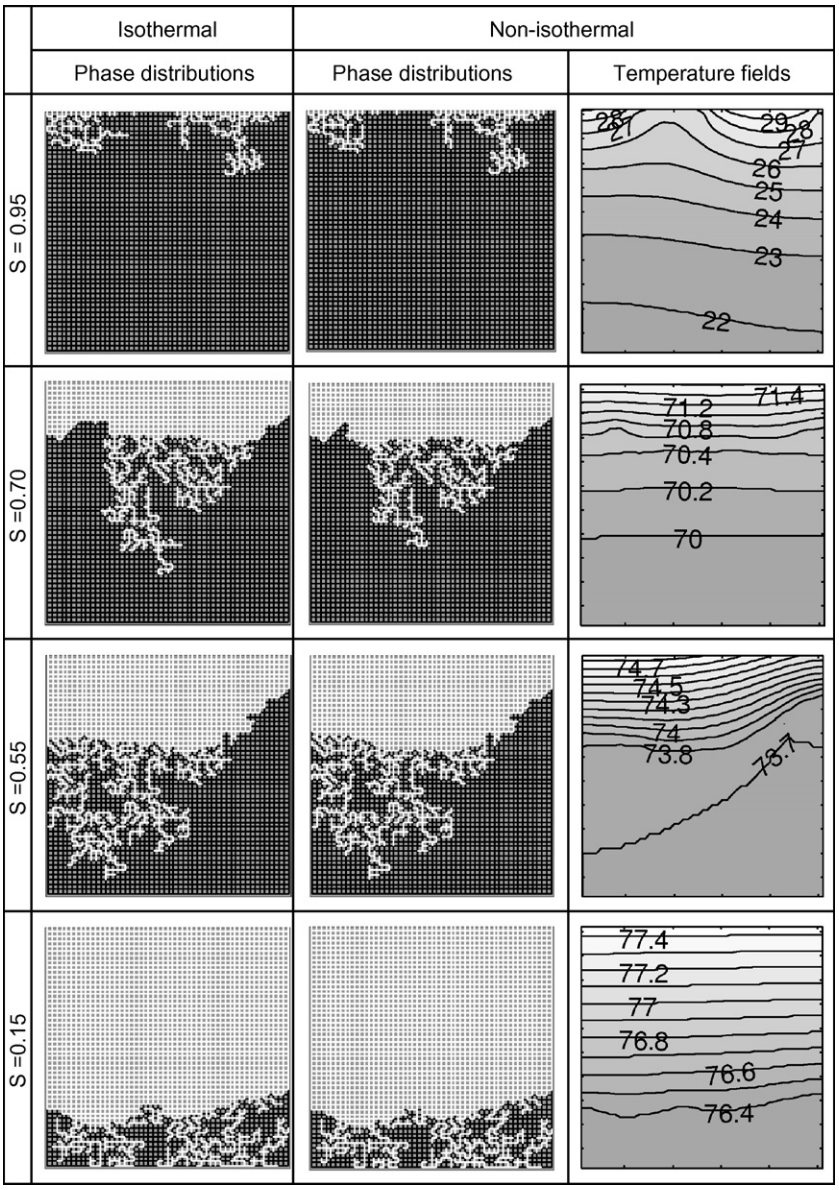

Fig. 14. Comparison of phase distributions for isothermal and non-isothermal simulations with a mono-modal pore network.

accommodated as long as the net phase change rate of a cluster does not require refilling of emptied throats. Due to low temperature gradients in the investigated cases, overall condensation rates are low and the committed error is shown to be negligible. Other ongoing work of the authors involves the application of the present model to contact drying where temperature gradients are significantly larger and in opposite direction [25]; in that case, the error on condensation rates can be important. Model improvement is under way for such more general applications. Additionally, the efficiency of the algorithm will be increased to simulate the drying of three-dimensional networks.

A further goal for the future is to develop a pore network drying model including all relevant transport processes, i.e. accounting also for viscous effects and gravity. A complementary project also aims to describe mechanical effects on the solid matrix, such as cracks and shrinkage, by the discrete network approach. Discrete modelling of porous media is seen as a fundamental method with a wider application range than classical continuum models. It offers a direct way to study the influence of microstructure on macroscopic behaviour, and it will help to develop highly specialized products and to integrate product and process optimization. Additionally, it will allow assessing continuous models and might provide a possibility to use structural information for computing effective parameters for these computationally more efficient models.

Acknowledgements

This work was financed by the German Research Foundation (DFG) in the frame of Graduate School 828 "Micro–Macro-Interactions in Structured Media and Particle Systems". The first author would like to express his special

thanks to Max-Buchner-Forschungsstiftung for its additional support.

References

[1] E. Sanchez-Palencia, Non-Homogeneous Media and Vibration Theory Lecture Notes in Physics, vol. 127, Springer-Verlag, 1980.
[2] M. Quintard, S. Whitaker, Transport in ordered and disordered porous media: volume-averaged equations, closure problems and comparison with experiments, Chem. Eng. Sci. 41 (14) (1993) 2537–2564.
[3] T.H. Vu, T. Metzger, E. Tsotsas, Influence of pore size distribution via effective parameters in a continuous drying model, in: Proceedings of 15th International Drying Symposium, Budapest, Hungary,Volume A, 20–23 August, 2006, pp. 554–561.
[4] M. Sahimi, Flow and Transport in Porous Media and Fractured Rock. From Classical Methods to Modern Approaches, VCH Verlagsgesellschaft GmbH-Weinheim, 1995.
[5] J.B. Laurindo, M. Prat, Modeling of drying in capillary-porous media: a discrete approach, Dry. Technol. 16 (9&10) (1998) 1769–1787.
[6] A.G. Yiotis, A.K. Stubos, A.G. Boudouvis, Y.C. Yortsos, Pore network model of drying of single-component liquids in porous media, Adv. Water Res. 24 (2001) 439–460.
[7] S.C. Nowicki, H.T. Davis, L.E. Scriven, Microscopic determination of transport parameters in drying porous media, Dry. Technol. 10 (4) (1992) 925–946.
[8] M. Prat, Percolation model of drying under isothermal conditions in porous media, Int. J. Multipha. Flow 19 (4) (1993) 641–704.
[9] J.F. Daian, J. Saliba, Determining a representative random pore-network for moisture sorption and migration in cement mortar, Int. J. Heat Mass Transfer 34 (8) (1991) 2081–2096.
[10] T. Metzger, A. Irawan, E. Tsotsas, Isothermal drying of pore networks: Influence of friction for different pore structures, Dry. Technol. 25 (2007) 49–57.
[11] J.B. Laurindo, M. Prat, Numerical and experimental network study of evaporation in capillary porous media. Phase distributions, Chem. Eng. Sci. 51 (1998) 5171–5185.
[12] J.B. Laurindo, M. Prat, Numerical and experimental network study of evaporation in capillary porous media. Drying rates, Chem. Eng. Sci. 53 (1998) 2257–2269.
[13] A.G. Yiotis, A.G. Boudouvis, A.K. Stubos, I.N. Tsimpanogiannis, Y.C. Yortsos, The effect of liquid films on the drying of porous media, AIChE J. 50 (2004) 2721–2737.
[14] M. Prat, On the influence of pore shape, contact angle and film flows on the drying of capillary porous media, Int. J. Heat Mass Transfer 50 (7&8) (2007) 1455–1468.
[15] L.A. Segura, P.G. Toledo, Pore-level modeling of isothermal drying of pore networks. Effect of gravity and pore shape and size distributions on saturation and transport parameters, Chem. Eng. J. 111 (2005) 237–252.
[16] L.A. Segura, P.G. Toledo, Pore-level modeling of isothermal drying of pore networks accounting for evaporation, viscous flow and shrinking, Dry. Technol. 23 (2005) 2007–2019.
[17] T. Metzger, A. Irawan, E. Tsotsas, Discrete modeling of drying kinetics of porous media, in: Proceedings of 3rd Nordic Drying Conference, Karlstad, Sweden, 15–17 June 2005.
[18] F. Plourde, M. Prat, Pore network simulations of drying of capillary porous media. Influence of thermal gradients, Int. J. Heat Mass Transfer 46 (2003) 1293–1307.
[19] H. Huinink, L. Pel, M.A.J. Michels, M. Prat, Drying processes in the presence of temperature gradients-pore-scale modeling, The Eur. Phys. J. E 9 (2002) 487–498.
[20] V.K. Surasani, T. Metzger, E. Tsotsas, Towards a complete pore network drying model: first steps to include heat transfer, in: Proceedings of 15th International Drying Symposium, Budapest, Hungary, Volume A, 20–23 August, 2006, pp. 125–132.
[21] M. Prat, Recent advances in pore-scale modeling for drying of porous media, Chem. Eng. J. 86 (2002) 153–164.
[22] W. Masmoudi, M. Prat, Heat and mass transfer between a porous media and a parallel external flow, application to drying of porous materials, Int. J. Heat Mass Transfer 34 (8) (1991) 1975–1981.
[23] A. Al-Futaisi, T.W. Patzek, Extention of Hoshen–Kopelman algorithm to non-lattice environments, Physica A 321 (2003) 665–678.
[24] T. Metzger, A. Irawan, E. Tsotsas, Remarks on the paper "Extension of Hoshen–Kopelman algorithm to non-lattice environment" by A. Al-Futaisi, T.W. Patzek, Physica A 321 (2003) 665–678, Physica A 363 (2006) 558–560.
[25] V.K. Surasani, T. Metzger E. Tsotsas, Influence of heat transfer on drying of capillary porous media: pore scale modeling, in: Proceedings of European Drying Conference AFSIA 2007, 24–25 May, 2007, Biarritz, France.